Materials & Design 218 (2022) 110677

Contents lists available at ScienceDirect

Materials & Design

journal homepage: www.elsevier.com/locate/matdes

Influence of aluminium powder aging on Directed Energy deposition

Adrien Da Silva [a,*], Filippo Belelli [b], Giorgia Lupi [b], Francesco Bruzzo [c], Benedikt Brandau [a,d], Lukas Maier [e], Alexander Pesl [e], Jan Frostevarg [a], Riccardo Casati [b], Elena Lopez [c], Alexander F.H. Kaplan [a]

[a] Department of Mathematics and Engineering Sciences, Luleå University of Technology, 97187 Luleå, Sweden
[b] Department of Mechanical Engineering, Politecnico di Milano, 1 Via Privata Giuseppe La Masa, 20156 Milano, Italy
[c] Fraunhofer, Institut für Werkstoff und Strahltechnik, Winterbergstraße 28, 01277 Dresden, Germany
[d] System Development Advanced Manufacturing, JENOPTIK Optical Systems GmbH, Göschwitzerstraße 25, 07745 Jena, Germany
[e] IMR – Metal Powder Technologies GmbH, Jessenigstraße 4, 9220 Lind ob Velden, Austria

HIGHLIGHTS

- Aging introduces both oxygen and hydrogen in aluminium powder.
- Oxygen affects the DED track geometry by reducing the surface tension of the melt.
- Hydrogen induces pores in the deposited material.
- Usage of aged aluminium powder in DED causes decreased mechanical properties.

GRAPHICAL ABSTRACT

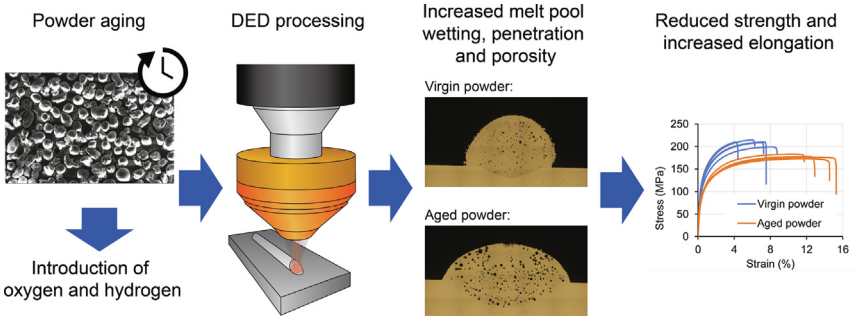

ARTICLE INFO

Article history:
Received 21 January 2022
Revised 11 April 2022
Accepted 17 April 2022
Available online 21 April 2022

Keywords:
Direct Metal Deposition
Laser Metal Deposition
Laser Powder Bed Fusion
Oxidation
Porosity

ABSTRACT

The use of aluminium alloys for Additive Manufacturing is of high interest for advanced geometries and lightweight applications. In Directed Energy Deposition, a powder stock is processed with a laser beam, which offers a high process flexibility. However, aging of the powder feedstock during storage or after recycling remains fundamentally challenging for aluminium alloys because of their sensitivity to oxidation and porosity. In order to investigate these effects, AlSi10Mg powder batches were aged in different conditions and processed by Directed Energy Deposition. The results showed that powder aging does not significantly change the particle size or morphology, but it introduces more oxygen and hydrogen in the powder. The oxidation of the particles reduces the laser beam absorbance of the powder and increases wetting of the melt pool, which affects the track geometry. A 3.5 to 4.2 times higher porosity was observed in the material deposited from aged powder, which are most likely hydrogen pores caused by the increased hydrogen content in the aged powder. The tensile properties of the parts built with aged powder showed 19.0% lower yield strength, 14.2% lower ultimate strength and 99.2% higher elongation, which are most likely the results of the coarser microstructure and increased porosity.

1. Introduction

Powder-based Additive Manufacturing (AM) has become widely used for advanced industrial applications requiring complex geometries. Aluminium alloys represent a consequent part of this production, offering a high benefit for lightweight applications within the aerospace, railway and automotive fields [1,2], one of the most commonly used aluminium alloys in AM being AlSi10Mg. Aluminium alloys are generally processed either by Laser Powder Bed Fusion (LPBF) [3–5] or by Directed Energy Deposition (DED) [6,7] depending on the size of the part and the geometrical

* Corresponding author.
E-mail address: adrien.da.silva@ltu.se (A. Da Silva).

https://doi.org/10.1016/j.matdes.2022.110677
0264-1275/

tolerances. The properties of AlSi10Mg built with LPBF have been widely investigated and show a porosity of 0.1% to 0.5%, a yield strength of 150 MPa to 280 MPa, an ultimate strength of 280 MPa to 426 MPa and an elongation of 2.2% to 17% as built [8–11]. The present study focusses on laser-powder DED, where the properties of AlSi10Mg seem to be lower than for LPBF with a porosity of 0.35% to 0.4% and an ultimate strength of 162 MPa [7], probably due to the larger scale and lower speed of the process which results in a lower cooling rate than in LPBF.

The main challenges for processing of aluminium are oxidation [12] and porosity [13] which induce various imperfections in the deposited material and weakens its mechanical properties. As it will be explained later on, most of these imperfections are caused by the powder being exposed to oxygen and hydrogen, which is more critical on powder than on bulk material due to their high surface to volume ratio. Exposition of oxygen and hydrogen can occur mostly during powder storage [14] or powder recycling [15].

Metal powder for AM is usually produced by inert gas atomisation, for aluminium alloys, nitrogen is often used as atomisation gas [16]. Metal ingots are melted in a crucible and the liquid is forced through a nozzle where it is atomised in small droplets by a high-velocity gas flow. The droplets solidify while falling and are collected in a chamber underneath [16,17]. The ingots are melted in vacuum and atomisation takes place in a sealed vessel where the material is in contact only with inert gas. Thus, oxidation and hydrogen pick up is extremely limited during powder atomisation.

Numerous studies have been performed on powder recycling of different materials for powder bed fusion processes and showed a slight increase of oxygen content in the powder (by 10 ppm to 90 ppm per reuse cycle), which did not significantly affect the porosity or mechanical properties of the parts [18–20]. Powder recycling for DED has been investigated with 316L stainless steel, the oxygen content was increased by approximately 1 ppm per reuse cycle and the particle size was substantially coarser, which caused a potentially higher porosity, a higher strength and lower elongation of the samples produced [15,21].

Similar effects can occur during powder storage. If a powder container has been opened, air containing oxygen and moisture can be introduced inside and the powder starts to age. This process takes a relatively long time but it can be simulated for a shorter time at higher temperature. It has been shown that aging of aluminium powder induces oxidation, which increases with temperature, moisture and aging time [14,22]. Processing of aged AlSi10Mg powder with 40 ppm increased oxygen content and 4 ppm extra moisture by LPBF was shown to result in an increased porosity, decreased yield strength, a potentially higher elongation, as well as a higher light absorption in the UV–visible range [9].

The exposition of aluminium powder to oxygen and hydrogen can have a certain impact on the powder properties and the DED process.

The presence of aluminium oxides (alumina) on top of the powder particles affects the laser absorbance of the powder. Pure aluminium is usually described as having an absorbance of about 5% and a reflectance of 95% [23], while alumina is partially transparent and its absorbance and reflectance cannot be described as surficial properties, they depend on the thickness of the alumina layer [24]. Thus, the laser beam light is partially reflected through the oxide layer before reaching the aluminium, which can reduce the overall absorbance of the powder particles. This potential reduction of the overall laser beam absorbance on the powder particles would result in a lower heat input in both the flying particles and the melt pool.

Once these particles are melted during processing, their oxides are transferred to the melt pool. It has been showed that oxides reduce the surface tension of liquid aluminium [25–27], which is likely to affect the melt pool shape and the final geometry of the tracks built with oxidised powder.

During processing, the oxide layer covering the melt pool can possibly affect the catchment and integration of powder particles in the melt pool. It has been observed that the oxide layer covering the melt pool prevents the powder particles from incorporating immediately, but the particles are yet caught on this layer and they can be incorporated at a slower rate [28,29]. The particles that do not incorporate usually ricochet at impact, which commonly happens when they land on the solidified metal [28]. This is an undesired effect as it reduces the efficiency of the process, decreases the deposition rate and contaminates the nearby environment.

Except from the oxygen, hydrogen is also a major cause of defects in aluminium, especially pores. Whereas there are other origins for pores in DED such as initial pores in the powder particles, gas entrapment and lack of fusion, hydrogen pores are the most predominant in aluminium alloys [30–32]. It can be explained by the solubility of hydrogen in liquid aluminium which decreases when the liquid cools down and suddenly drops by a factor of 70 during solidification [33–36]. Most of the hydrogen diluted in the liquid at high temperature is forced to regain its gaseous form when the liquid cools down and its hydrogen solubility decreases, this forms hydrogen bubbles that will become pores once the aluminium is solidified [13,33,37]. Hydrogen pores are recognisable by their spherical shapes of various sizes and their even distribution in the solidified metal [37].

Pores have a negative impact on the mechanical properties. A first reason is due to the decrease of working area for the same outer geometry, meaning that the load will apply to a lower amount of material, inducing higher stress. Another reason is the stress concentration around the pores which initiates cracks and leads to a premature rupture. In tensile conditions, it has been showed that for each percent of porosity, the yield strength, ultimate strength and elongation of various aluminium alloys was reduced by 4–7.5%, 0.5–4% and 1.6–7% respectively [38–40]. The porosity of aluminium is even more crucial for fatigue properties where it reduces significantly the fatigue life of the parts [41,42].

Due to the many undesired effects on aluminium powder-based AM that can be induced by oxygen and hydrogen in the powder, it appears necessary to conduct a comprehensive study to investigate the course of phenomena that leads to the mechanical properties of aluminium parts. This study will be conducted on DED since it is a macro-process, which facilitates the observations and measurements of the phenomena investigated. The goal of the present research is to compare all of these effects to the oxygen and hydrogen contents in the powder in order for the results to be generalizable to any atomised, aged or recycled AlSi10Mg powder.

2. Methodology

2.1. Powder aging and analysis

In order to introduce oxygen and hydrogen in nitrogen atomised AlSi10Mg powder, aging treatments were performed at high temperature in air inside an oven. Three powder aging conditions were investigated: virgin powder as received, aged powder at 400 °C for 48 h and aged powder at 400 °C for 96 h. The powder was aged in large trays with a powder thickness of few millimetres and was mixed every 24 h to guarantee a homogeneous aging. In order to limit the uncertainty of measurement in subsequent analysis, the same aging procedure was applied to five batches of powder (Batch 1, 2, 3, 4 and 5) that had relatively similar particle size distributions (PSD). Thus, each analysis step was performed on four powder batches for each of the three aging conditions, providing

more statistical data for the evaluation. Before processing, the following analysis were conducted on the twelve batches of powder:

- Laser diffraction particle size analysis to measure the PSD
- Hot gas extraction analysis to measure the oxygen and hydrogen contents with a LECO ONH836 analyser
- Scanning Electron Microscopy (SEM) observations of the powder
- Laser beam absorbance measurement done with a spectrometer in an integrating sphere [43–46].

For the laser beam absorbance measurements, a sample of 10 mL of powder was placed in a Suprasil® 3001 quartz cuvette located on one side of the integrating sphere. A spectrometer composed of two light sources was placed on the other side of the integrating sphere, illuminating the powder sample with a deuterium lamp for the wavelength range of 175 nm to 400 nm and a halogen lamp covering the wavelengths from 400 nm to 3300 nm. The light reflected on the powder was then reflected multiples times inside the integrating sphere until reaching the detector. The total reflected power on the powder was subtracted from the power of the initial light beam in order to measure the power absorbed on the powder and calculate the absorbance value for each wavelength. The absorbance measurements were performed for the range of wavelengths from 330 nm to 1560 nm (which includes the wavelengths of the laser used) with an accuracy of ± 0.08 nm in the UV–visible range and ± 0.32 nm in the near IR range. Please note that since a high number of powder particles were placed in a cuvette, multiple reflections between powder particles induce a higher overall absorbance, which is comparable with the absorbance of a powder bed.

2.2. Processing and analysis of single DED tracks

Each of the twelve powders from Batch 1, 2, 3 and 4 was dried in the oven at 100 °C for one hour, then processed with DED according the setup shown in Fig. 1. For these depositions, a COAX14-V5 coaxial powder nozzle (provided by Fraunhofer IWS) and a 15 kW Ytterbium fibre laser were used. The laser beam was transported through a 400 µm optical fibre to the optics, that consisted of a collimating mirror and a focusing mirror with focal lengths of 150 mm and 250 mm respectively. The laser beam was defocussed by 40 mm on the substrate, which resulted in a laser spot size of 4.4 mm. More details about the setup and the laser beam profile can be found in reference [47]. 8 cm long tracks were deposited on separate AW–6082 substrates (10 mm thick). The parameters were kept the same for all depositions (Single tracks in Table 1).

A Phantom V1610 high-speed imaging (HSI) camera was used to record the process (Fig. 1). The processing area was illuminated with two CW illumination lasers with a maximum power of 45 W each and a wavelength of 810 nm. A band-pass filter of the same wavelength was placed in front on the camera optics to filter out the laser scattered light and most of the process light. The camera optics consisted of a Nikon AF Micro-Nikkor ED 200 mm s/4D IF lens with magnification rings of 48 mm total length. The camera was recording at a speed of 78 000 fps, with a frame size of 512 × 320 pixels, a shutter time of 1 µs and an aperture of 16. The spatial resolution of the videos was 23.1 µm per pixel.

The HSI videos were used to analyse the powder particles that do not integrate in the melt pool and ricochet on the surface. To that end, a single particle tracking procedure was applied to the videos with the software TrackMate [48,49]. Each video was 20 ms long (1560 frames) and was played in reverse in the software. The detector used was a difference of Gaussians (DoG), with an estimated blob diameter of 4 pixels, a search radius of 5 pixels and a maximum frame gap of 2 frames. Different thresholds were applied to: (i) the particle detection in order to avoid background noise, (ii) the particle paths in order to remove the static particles

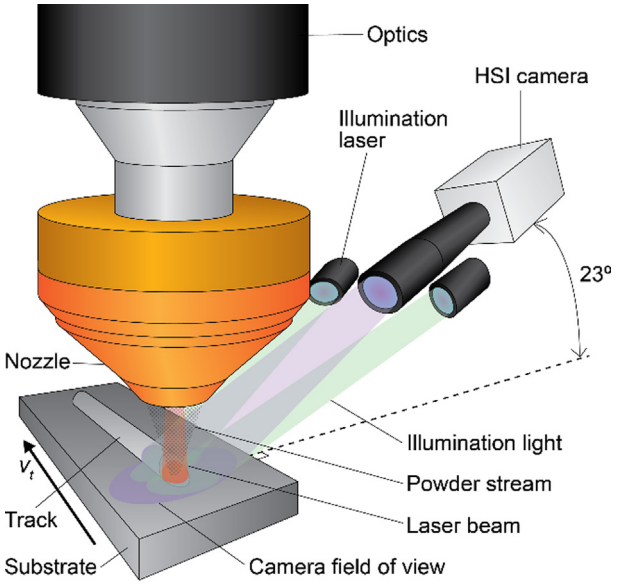

Fig. 1. Experimental setup for the deposition of single DED tracks with high-speed imaging recording.

Table 1
Parameters for the deposition of single tracks and larger structures (optimised for virgin powder).

	Single tracks	Larger structures
Laser spot size (mm)	4.4	1.6
Laser power (W)	3000	2060
Travel speed v_t (m/min)	0.5	Fill: 0.6 Contours: 0.4
Powder feed rate (g/min)	4.0	2.8
Argon carrier gas flow (L/min)	10	12
Argon shielding gas flow (L/min)	15	15

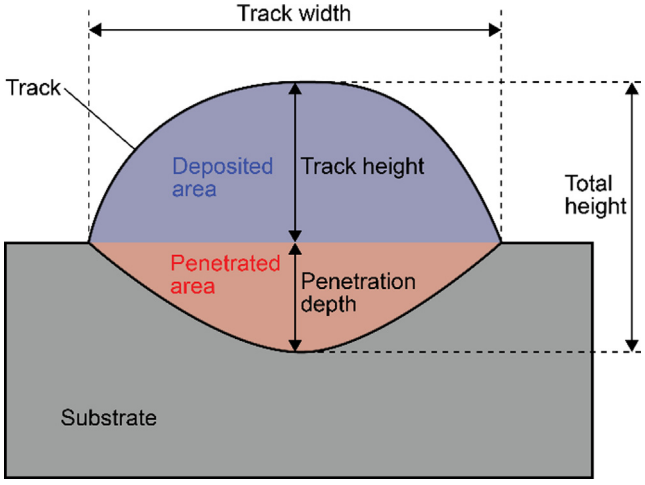

Fig. 2. Schematics of the track geometry measurement.

Table 2
PSD of the powders investigated in different aging conditions.

	Condition	D10 (μm)	D50 (μm)	D90 (μm)
Batch 1	Virgin	48.1	65.7	89.3
	Aged 48 h	51.3	68.4	91.6
	Aged 96 h	51.8	68.9	92.4
Batch 2	Virgin	49.3	67.9	93.3
	Aged 48 h	49.0	68.4	94.8
	Aged 96 h	51.1	71.3	99.0
Batch 3	Virgin	52.0	72.2	101.0
	Aged 48 h	54.0	74.9	104.0
	Aged 96 h	52.5	73.8	104.0
Batch 4	Virgin	50.0	69.9	97.2
	Aged 48 h	51.7	71.2	97.9
	Aged 96 h	50.2	70.2	97.5
Batch 5	Virgin	47.9	67.7	102.0
	Aged 96 h	53.3	68.5	98.5

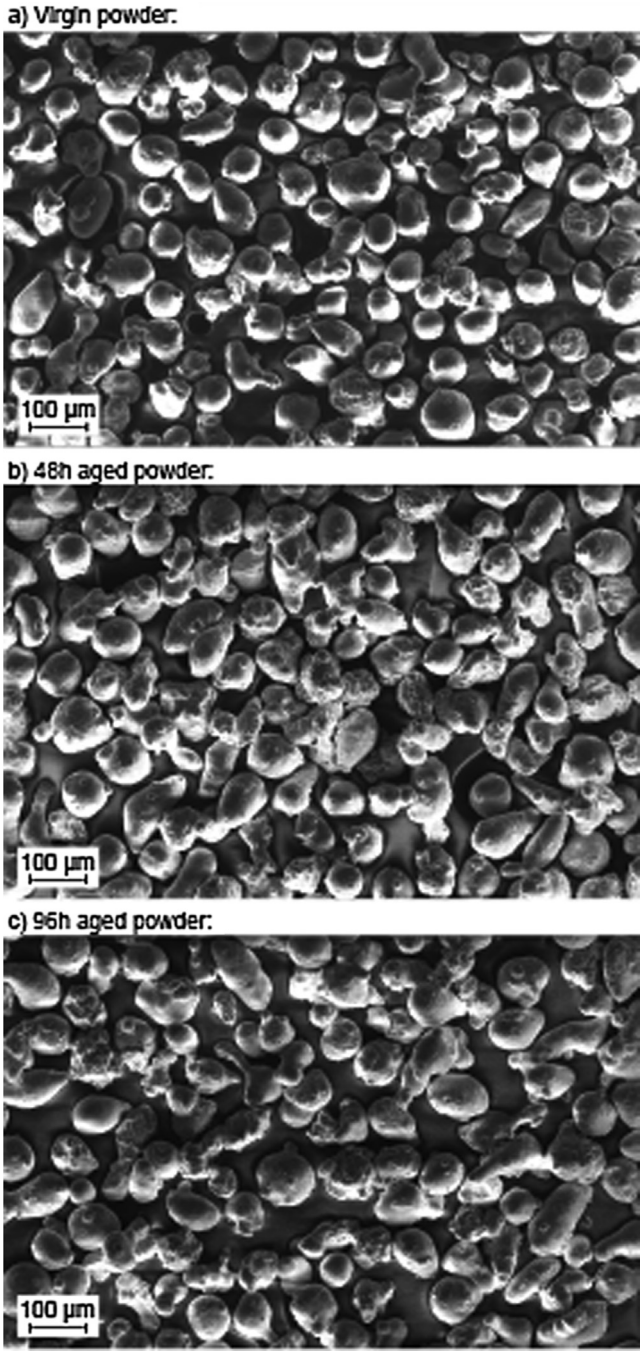

Fig. 3. SEM views of Batch 4 powders at different aging conditions.

landed on the substrate and the particles in the powder stream that incorporate in the melt pool.

After processing, lateral cross sections were cut at 20 mm from the beginning of each DED track and observed with a light optical microscope (LOM) to analyse the track geometry, the penetration in the substrate and the inner-track porosity. Two different methods were applied to measure the track geometry and the penetration: 1-dimensional measurements of width, height and penetration, and 2–dimensional measurement of the areas above the substrate and below the substrate. In the cross–sections, the area above the substrate represents the volume added from the powder feedstock, while the area below the substrate represents the volume of substrate melted, representative of the penetration (Fig. 2). The resolution of the micrographs was 0.48 μm per pixel. The porosity analysis was carried out with a Matlab® script that recognised every pore bigger than 4 pixels (about 1 μm diameter). The size of each pore was extracted and the total percentage of porosity was calculated. Please note that the porosity analysis in a cross section is a reliable technique to measure the percentage of porosity in the material (if the number of pores is high), but not the actual pore size, since not all the pores are cut at their maximum diameter.

2.3. DED Manufacturing of larger structures and mechanical testing

Larger structures were built by DED with a commercial system using two different powders from Batch 5: virgin powder and powder aged at 400 °C for 96 h. For each powder, six blocks of 12 × 12 × 60 mm were built horizontally. The DED machine was a DMG Lasertec 65 3D Hybrid, with a COAX14-V5 coaxial powder nozzle and a 4 kW diode laser composed of four 1 kW modules with wavelengths of 940 nm, 980 nm, 1020 nm and 1060 nm. The structures were built on an AW–6082 substrate (10 mm thick) fixed on a copper plate with active internal water cooling. Since these structures were built by a different system than for the single tracks, the parameters used are slightly different, as shown in Table 1. The hatch distance was 1.5 mm, which represents 40% of overlap between two consecutive tracks under regular conditions (with virgin powder). The AlSi10Mg powder used for these structures (Batch 5) had a similar PSD than for the four other batches used for single tracks.

For each of the two powders, five tensile specimens and one lateral cross-section were extracted out of the six deposited volumes. Five specimens were tested for the virgin powder and four for the

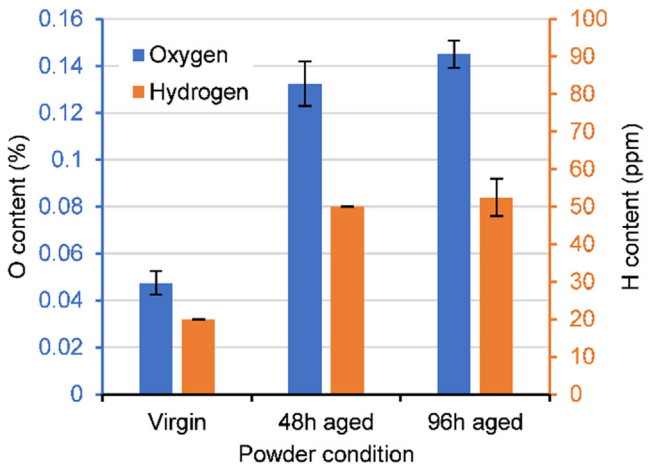

Fig. 4. Oxygen and hydrogen contents measured in the powder by ICP-MS as a function of the aging time at 400 °C, where each point is the average value measured for Batch 1, 2, 3 and 4.

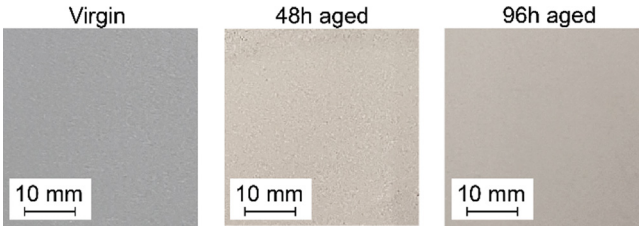

Fig. 5. Photographs of the powder batch 4 showing the difference of colour at different aging conditions.

96 h aged powder, one was broken during machining. The tensile tests were conducted according to ASTM E8/ E8M-13a standard. The tensile specimens were cylindrical with a testing length of 22 mm and a testing diameter of 3 mm, they were treated with a stress-relief treatment at 300 °C for 2 h before testing. The tensile tests were performed at a crosshead speed of 1 mm/min and the displacement was measured with an extensometer. Macroviews of the cross-sections were captured by LOM (with a resolution of 5.55 µm per pixel), which were used to measure the structural porosity inside the blocks (the minimum pore diameter detectable was 13 µm). Magnified views of the microstructure were taken with a SEM.

3. Results

3.1. Powder properties during aging

The powders investigated for the deposition of single tracks (Batch 1, 2, 3 and 4) and bigger structures (Batch 5) at virgin and aged conditions (according to the procedure described in section 2.2) were analysed. Table 2 shows the PSD of these powders, where it can be noticed that aging does not have any considerable effect on the particle size. The minor fluctuations of size between different aging conditions are most likely due to statistical deviation since they do not follow any clear trend as a function of the aging time. The following powder analysis will focus mostly on the powder batches 1, 2, 3 and 4. SEM observations of the different powders showed a similar morphology independently from the aging condition, as it can be seen in Fig. 3 for Batch 4.

The main effect of powder aging is therefore not in the particle size or morphology, but rather in the chemical composition. A hot gas extraction analysis of the batches 1, 2, 3 and 4 in three different aging conditions allowed to measure the oxygen and hydrogen contents in the powders, as plotted in Fig. 4. Both the oxygen and hydrogen levels in the powder increase in similar proportions when aging the powder, following a logarithmic-like tendency, the oxygen content being always significantly higher than the hydrogen content.

The oxidation of the particles surface affects their apparent colour, as shown in Fig. 5. The colour changes from grey at virgin state to a brighter beige at aged conditions, meaning that the powder absorbs and reflects certain wavelengths differently depending on its oxide layer. This observation motivated the conduction of a light absorbance measurement for the wavelengths emitted by the lasers used.

As it can be seen in Fig. 6a, the light absorbance measurements performed on the powders shows that both the 48 h aged and the 96 h aged powders follow a similar absorbance tendency, which is relatively different from the virgin powder. Above a wavelength of 450–500 nm, the absorbance of the aged powder is lower than the one of the virgin powder, while the opposite applies below 450–500 nm. The powder laser beam absorbance can be compared to the oxygen content in the powder (cf. Fig. 4), as shown in Fig. 6b.

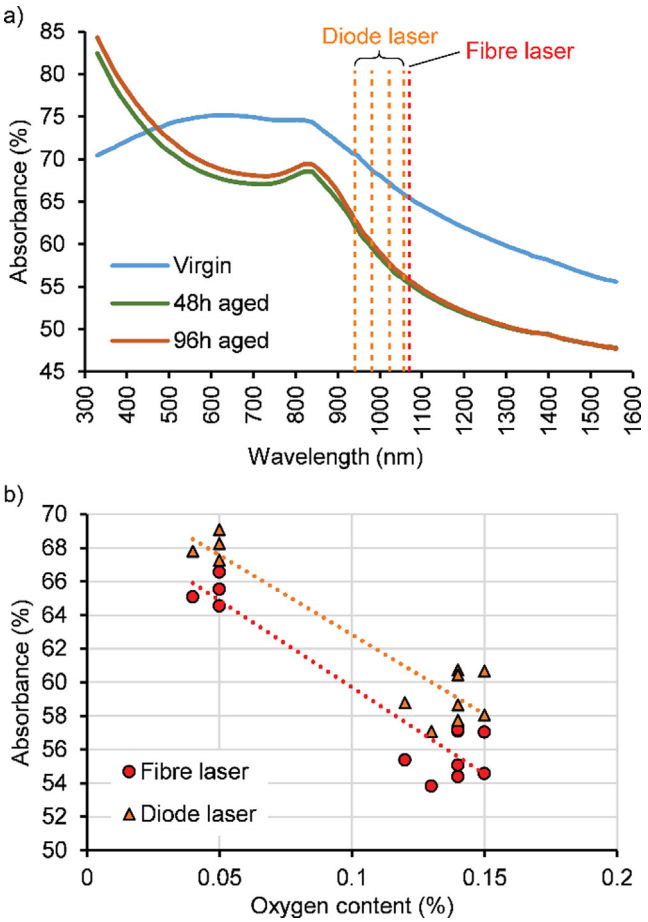

Fig. 6. a) absorbance of the powder as a function of the illumination wavelength, averaged over the values measured on Batch 1, 2, 3 and 4, b) absorbance measured on the powder for the two lasers employed for DED processing as a function of the oxygen content measured in the powder, where the values for the diode laser were the average of the 4 wavelengths used by each of the laser modules.

More details on the powder absorbance can be found in a related study [50].

It can be observed that the absorbance of the powder for both lasers used is decreased with increased oxygen content. Please note that due to the data points being grouped into two main clusters (for the virgin powder and for the aged powder), it is not possible to conclude on a potential proportionality or any other relation between the absorbance and the oxygen content.

3.2. Single-track properties

Single tracks were deposited by DED using the twelve powders previously analysed at different aging conditions (from Batch 1, 2, 3 and 4) while a HSI camera was recording the process. Fig. 7 shows the results of particle tracking with the corresponding trajectories of the particles that ricochet at impact. Most of these particles ricochet from the front of the melt pool and less often from the back. The particles are considerably slower after ricocheting, with a velocity of 0.56 m/s to 3.96 m/s, while in the powder stream, the particles have a velocity of approximately 13 m/s [47]. As it can be seen in Fig. 8, there is no clear trend relating the number of ricocheting particles to the oxygen content in the powder. The data points are relatively dispersed and do not imply any tendency. Thus, it appears that the aging of the powder does not affect the overall ability of the particles to incorporate in the melt pool.

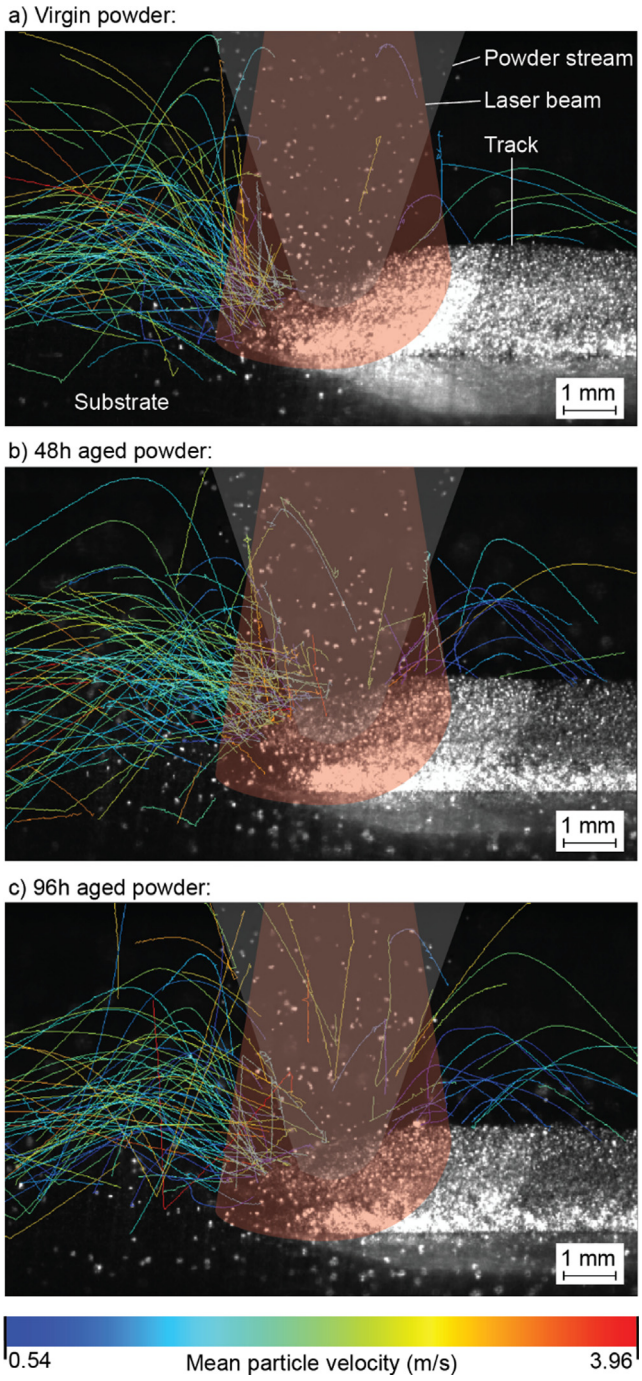

Fig. 7. Frames of HSI imaging captured during the DED processing of single tracks using batch 2 powders at different aging conditions, including results of particle tracking where each coloured line represents the trajectory and velocity of a ricocheting particle detected under 20 ms.

The single tracks built with different powder aging conditions showed different morphologies, as it can be observed in Fig. 9. The tracks become flatter, wider and show a deeper penetration in the substrate with increased powder aging. It is also possible to observe a significantly higher porosity in the tracks built with aged powder.

The dimensions of the tracks were measured and compared to the oxygen content in the powder, as it can be seen in Fig. 10. When considering the average 1-dimensonal measurements of the tracks (Fig. 10a) from the virgin condition (0.048% oxygen) to the aged conditions (0.138% oxygen), the width is increased by

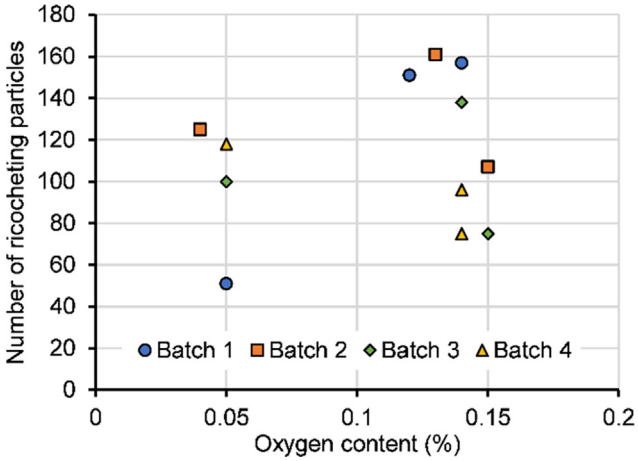

Fig. 8. Number of ricocheting particles recorded during 20 ms as a function of the oxygen content in the powder.

33%, the height is decreased by 19% and the penetration is increased by 55%, while the total height remains constant. On the other hand, when considering areal measurements of the tracks (Fig. 10b) from virgin to aged condition, the deposited area potentially decreases by 2% (within the dispersion of data), the penetrated area increases by 118% and the total melted area (deposited area + penetrated area) increases by 20%.

The inner porosity of the tracks was analysed based on the LOM views of the cross-sections, as shown in Fig. 11. The percentage of porosity increases significantly from virgin powder (1.91%) to aged powder (8.00% and 6.67% for the 48 h aged powder and 96 h aged powder respectively), which represents an average increase of porosity of 284% for a hydrogen increase of 156% (Fig. 11a). The pore size is also affected by powder aging (Fig. 11b), where the average pore size increases from 7.0 μm with virgin powder to 13.0 μm and 12.3 μm with 48 h aged and 96 h aged powders respectively. As the error bars show on this graph, there is also a higher number of larger pores when processing aged powder compared to with virgin powder.

3.3. Structural properties

Larger structures were built by a commercial DED system with virgin and 96 h aged powders from Batch 5. Six horizontal blocks were built with each powder, as shown in Fig. 12. It is possible to notice a clear change of colour between these blocks, where the blocks built with 96 h aged powder are darker than the ones built with virgin powder. The blocks built with aged powder also showed a significantly lower lateral surface quality. In the cross-sections of the blocks (Fig. 13), the porosity measurements showed an increase of porosity of 91.5% from the structures built with virgin powder to the ones built with 96 h aged powder. It can also be noticed that the diameter of the pores is increased by 38.7% and that most of the biggest pores in the blocks built with 96 h aged powder seem to be located close to the upper surface and the lateral surfaces.

As shown in Fig. 14, the microstructure is composed of fine primary α-aluminium cells (bright) surrounded by an abundant segregation of α-Al-Si eutectic phase mixture (dark) at the cell boundaries. A coarser microstructure is noticeable in the SEM images collected on the cross-section of the blocks produced with 96 h aged powder compared to virgin powder.

Tensile tests were performed using specimens machined out from the blocks, the results are displayed in Fig. 15. The tensile

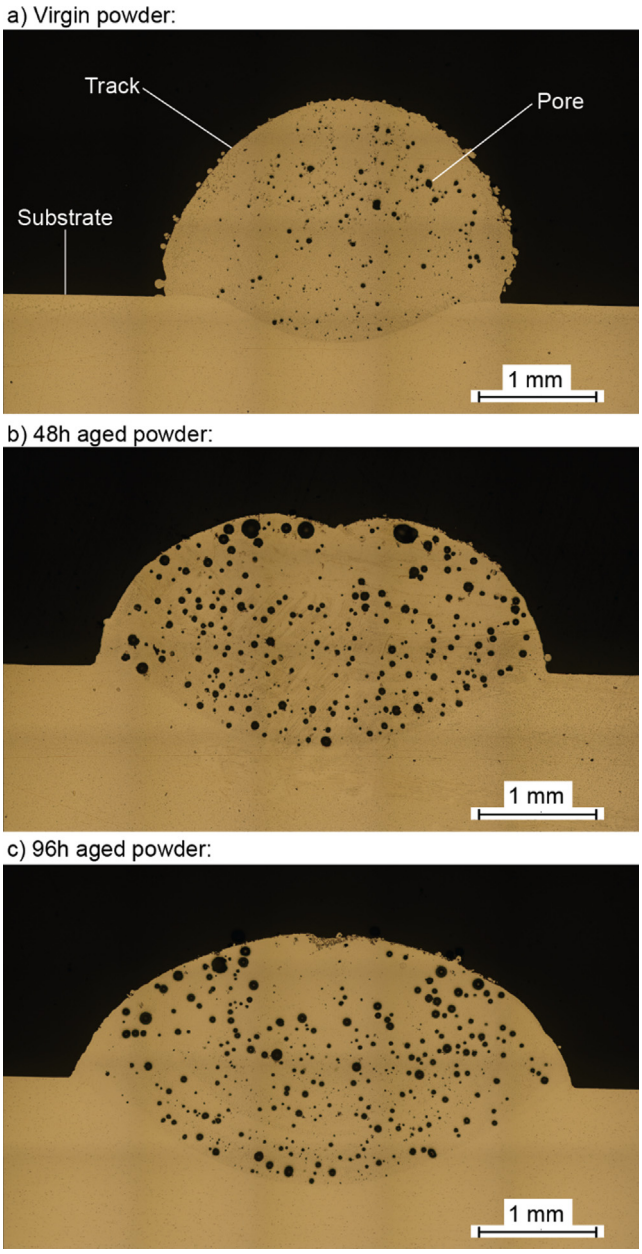

Fig. 9. LOM views of the single tracks cross-sections built with Batch 4 at different aging conditions.

properties of the specimens built with these two powders are very distinct. In average, when using 96 h aged powder compared to virgin powder, the yield strength and the ultimate strength are decreased by 19.0% and 14.9% respectively, while the elongation is increased by 99.2% (Table 3).

4. Discussion

Based on the results obtained in this study, different correlations can be established between the powder properties, the melt pool, the track and the structural properties. All aspects discussed in this section are illustrated in Fig. 16.

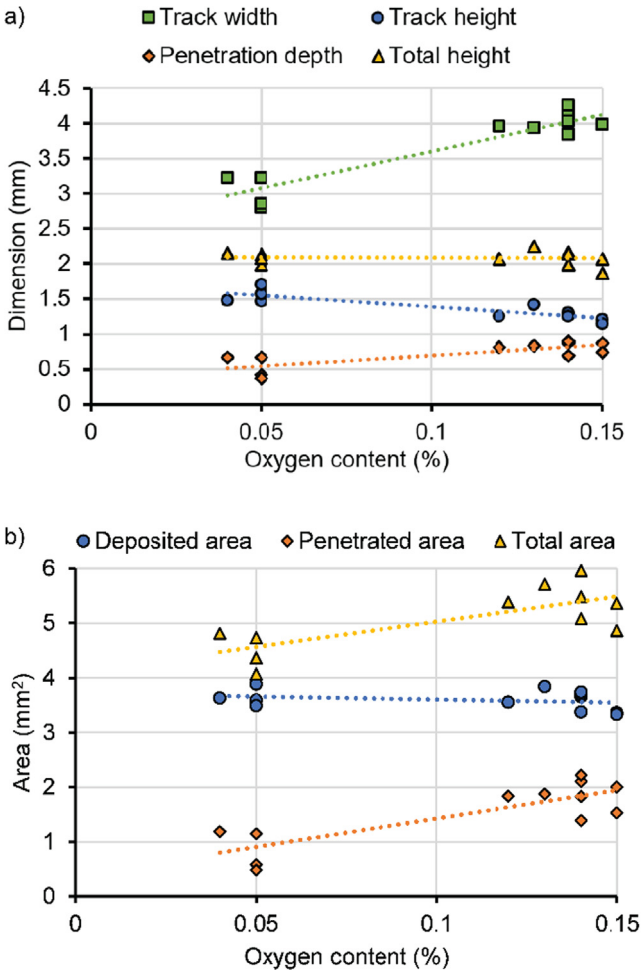

Fig. 10. a) 1-dimensional measurements, and b) areal measurements of the tracks extracted from the LOM views of the cross-sections of the single tracks (as described in Fig. 2) built with powders at different aging conditions from Batch 1, 2, 3 and 4.

4.1. Powder aging

The powder analysis after aging showed an increase of both the oxygen and hydrogen contents in the powder (Fig. 4), which is in accordance with previous studies [9,14,22]. For all powders, the oxygen content was significantly higher than the hydrogen content by a factor of 20 to 30. Oxidation is due to the dioxygen content in the air (21%) and the humidity content, while the hydrogen pick up by the powder is mostly due to the humidity, the hydrogen content in the air being only about 0.6 ppm [51]. There could also be a causal link between the oxygen and hydrogen contents in the powder. It is possible that the oxidised surface of the aged powder particles attracts more water molecules via hydrogen bounds (between the O of oxides and the H of water), which could be the reason for the higher moisture contents measured in aged AlSi10Mg powders in [9].

The oxide layer on aluminium surfaces is generally few nanometres thick [12,52–54] which did not change the size or the morphology of the powder (Table 2 and Fig. 9), which was confirmed by [9]. However, the oxide layer was shown to have an effect on the powder absorbance (Fig. 6). The laser beam light was most likely reflected more when going through a thicker oxide layer, resulting in a lower powder absorbance, which induces a lower heat input from the laser beam.

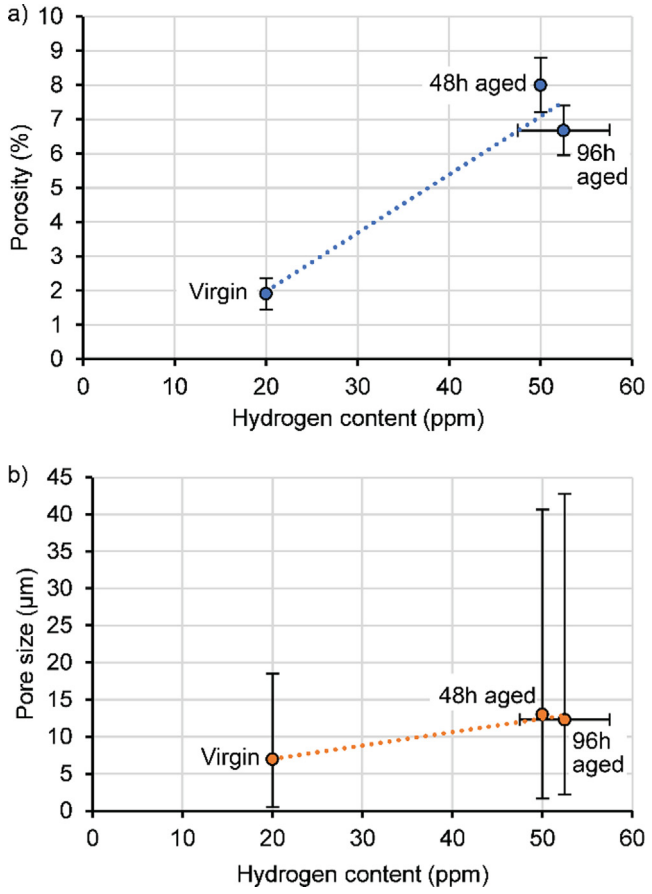

Fig. 11. a) Inner-track porosity measured on the cross-section of the single tracks built with powders at different aging conditions from Batch 1, 2, 3 and 4, and b) associated pore size where the vertical error bars represent the average standard deviation of pore size within one cross-section.

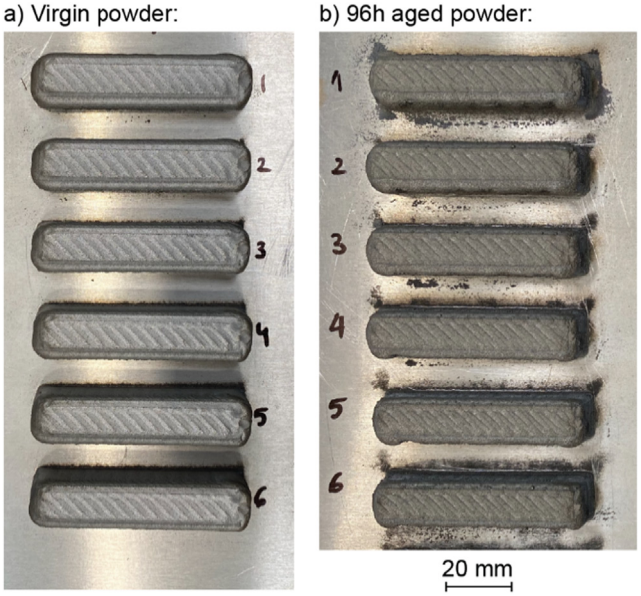

Fig. 12. Photographs of the blocks built with virgin powder and 96 h aged powder from Batch 5.

4.2. Oxygen content and track geometry

As it can be noticed in Fig. 7 and Fig. 8, the incorporation of powder particles in the melt pool is not affected by the higher oxygen content of the powder. The particles most likely incorporate as well even through a potentially thicker oxide layer covering the melt pool. It means that there was no extra loss of powder and that the same volume was deposited independently from the powder aging condition. This is in correlation with what was measured in the track cross-sections (Fig. 10b) where the deposited area is relatively constant regardless of the oxygen content in the powder.

However, even though the deposited volume is unchanged, the geometry of the tracks is different for different powder aging conditions (Fig. 9). The tracks exhibit a lower height and a larger width with increased oxygen content in the powder (Fig. 10a), which indicates that the surface tension of the melt pool was probably decreased. One potential reason could be a higher melt tempera-

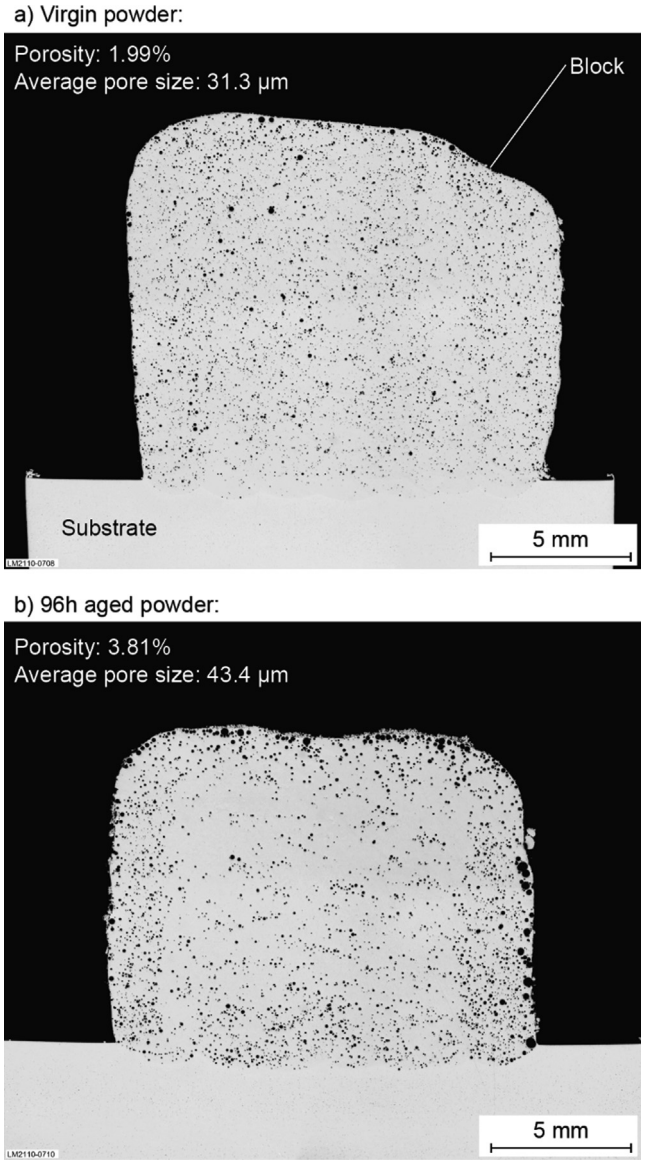

Fig. 13. LOM views of the cross-sections of the blocks built with virgin powder and 96 h aged powder from Batch 5.

ture due to oxidation. However, even though the aged powders contained more oxygen than the virgin powder, the reaction of oxidation, which is exothermic [55], occurred before processing, during aging in the oven. During the DED process, the aged powder is already oxidised and any extra oxidation occurring during processing (due to the contact between the melt and the dioxygen in the air) presumably happens in the same measure as when processing virgin powder. Thus, it appears very unlikely that the oxidation occurring during processing could differ between virgin and aged powder and result in different heat inputs in the melt pool. Instead, the decrease of surface tension is very likely due to the increased oxygen content, as shown in previous studies [25–27]. It is also

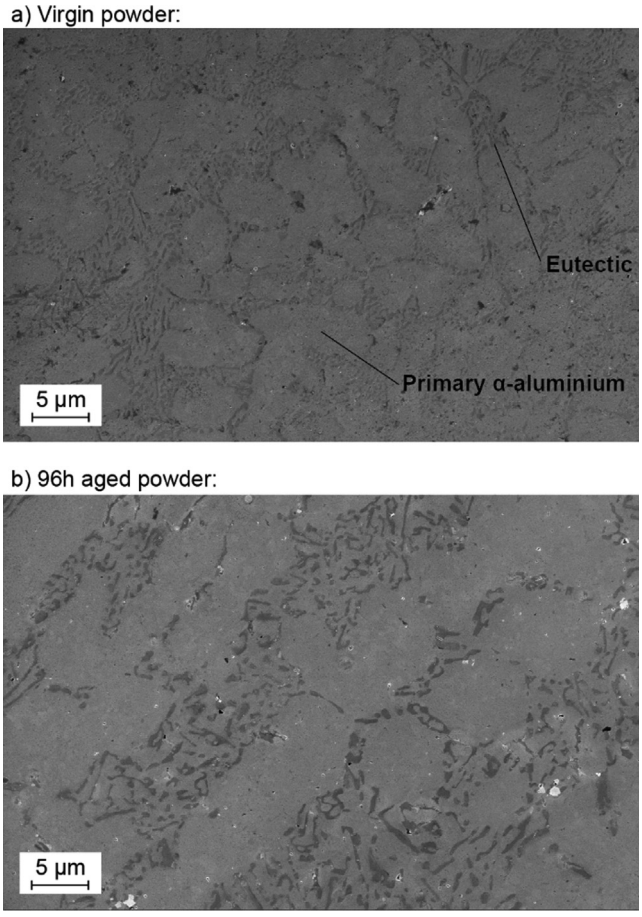

Fig. 14. SEM views captured at the same location in the cross-sections of the blocks built with virgin powder and 96 h aged powder from Batch 5.

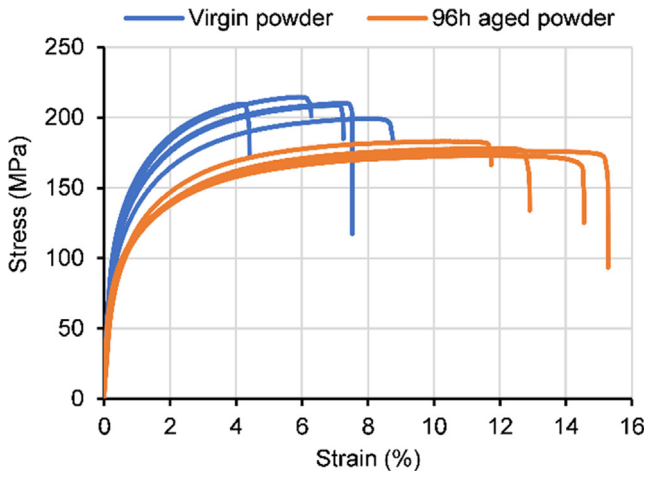

Fig. 15. Results of the tensile tests conducted after a stress-relief treatment on specimens built with virgin powder and 96 h aged powder from Batch 5.

Table 3
Structural properties of the deposited material correlated to the oxygen and hydrogen contents in the powder (Batch 5).

	Virgin powder	96 h aged powder
Oxygen content (%)	0.05	> 0.15*
Hydrogen content (ppm)	20	40
Structural porosity (%)	1.99	3.81
Yield tensile strength (MPa)	106.8 ± 7.4	86.5 ± 4.0
Ultimate tensile strength (MPa)	208.6 ± 5.2	177.5 ± 3.6
Tensile elongation (%)	6.84 ± 1.44	13.63 ± 1.41

*Out of the calibration range but expected to be relatively close to 0.15% in accordance with the measurements performed on other powders (Fig. 4).

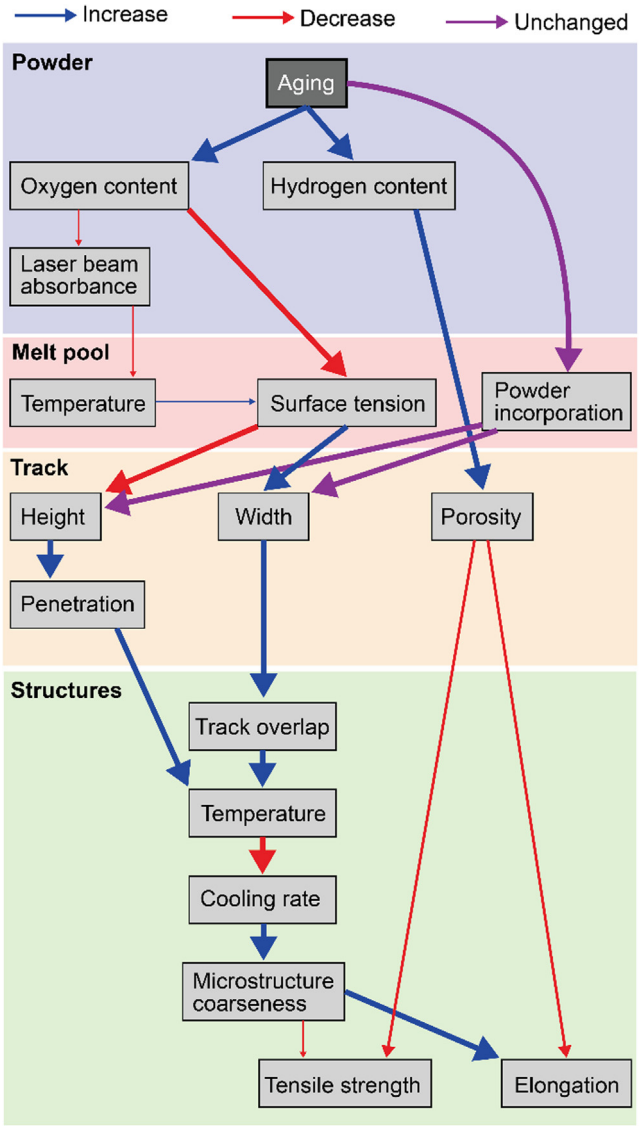

Fig. 16. Representation of the relations between the phenomena induced by powder aging, where the thickness of the arrows represents the importance of the correlation.

important to note that the penetration in the substrate is higher with increased oxygen content. It can not be due to a higher temperature since the laser beam absorbance does not increase, as shown in Fig. 6 the absorbance even decreases with increased oxygen content. The higher penetration could be due to the lower track height. As shown in Fig. 10a, the total track height is always the same with a value of 2.1 mm, meaning that when the track height decreases, the penetration increases by the same amount. It appears very likely that with the parameters chosen the laser beam always induces a 2.1 mm deep melt pool. The decreasing surface tension of the melt pool due to the increased oxygen content causes a reduced height of the melt pool above the substrate. At the same time, the melt pool depth in the substrate increases, resulting in an almost identical total height of 2.1 mm.

Building larger structures with aged powder using parameters optimised for virgin powder possibly has an effect on the heat accumulated in the structure. First, processing of aged powder induces a higher penetration in the previous layer, which most likely leads to higher temperatures in the previous layers. Secondly, for the same hatch distance, the increased track width caused by powder aging results in an increased track overlap, as shown in Fig. 17. In Fig. 10a the track width is increased by 33% from virgin to aged powder, meaning that a track overlap of 40% with virgin powder would become 54.9% with aged powder. This increase of overlap is very likely to lead to higher temperature in the preceding track. Both the increase of penetration and the increase of track overlap might then induce a higher temperature in the structure being built.

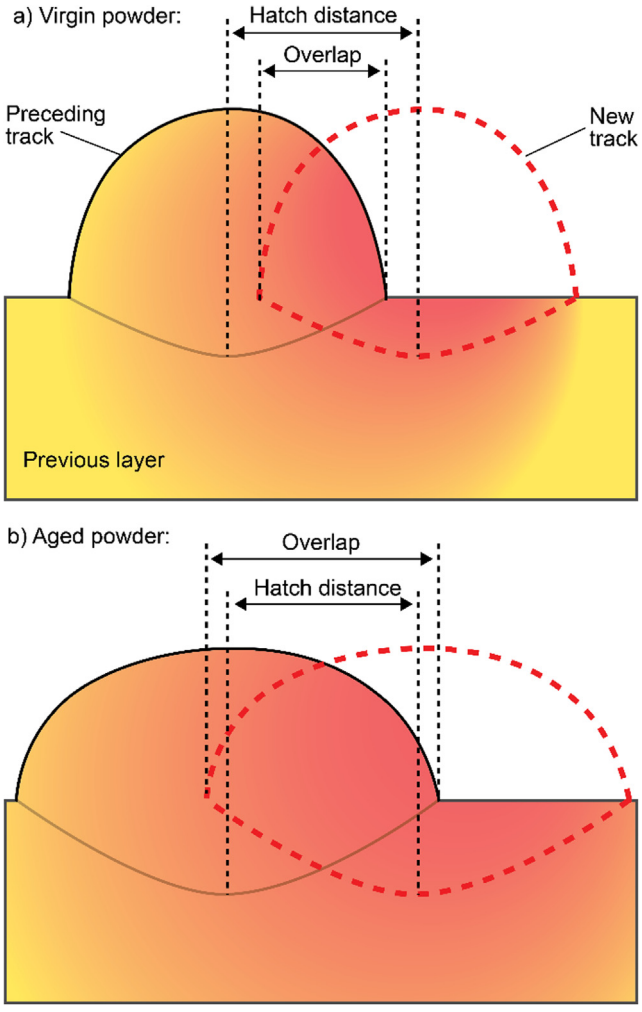

Fig. 17. Effect of increased overlap and penetration on the temperature of the structures built with virgin and aged powder.

Due to the increase of temperature in the nearby structure when processing aged powder, the material is most likely submitted to more heat cycles and cools down slower. This lower overall cooling rate leads to a coarser microstructure, as observed in Fig. 14. When using aged powder, the material becomes less quenched as when using virgin powder, which might result in a slightly lower yield strength and ultimate strength, as well as in a higher elongation, as shown in Fig. 15.

4.3. Hydrogen content and porosity

The pores observed in the cross-sections in Fig. 9 and Fig. 13 are spherical indicating that they are gas pores. In the cross sections from large structures no pores pattern is clearly visible (Fig. 13), indicating that the pores are forming within each track and not due to defects formation between different tracks or layers. The porosity increases with aging (Fig. 11), which means that it is caused either by the hydrogen or the oxygen introduced in the powder. According to previous studies, hydrogen is the main cause for porosity in aluminium alloys where a few tens of ppm of hydrogen can induce a significant porosity, and no correlation between oxygen and porosity has been established yet [13,33,37]. Thus, it appears very likely that the pores investigated in the present research are due to hydrogen rather than oxygen. Moreover, it appears that with aged powder, the bigger pores are concentrated mostly at the periphery of the single tracks (Fig. 9) and at the periphery of the blocks (Fig. 13). One explanation for this phenomenon could be that small pores merge into bigger pores when migrating towards the surface during mixing.

The structural porosity measured in the blocks built with 96 h aged powder is relatively lower than the inner-track porosity measured in single tracks (Fig. 11 and Fig. 13). It is likely due to the different systems used for the deposition of single tracks and blocks and the different resulting parameters used for the depositions (Table 1). In each case (for the deposition of single tracks and blocks), as well as in the literature, the porosity of AlSi10Mg increases with powder aging [9].

The increased porosity in the structures built with aged powder compared to with virgin powder is most likely responsible for most of the decrease of yield strength and ultimate strength in the specimens during tensile testing, as it has been showed in other studies [38–40]. A minor part of this decrease of strength is possibly due to the coarser microstructure, as mentioned in the previous section. The decreased of elongation caused by the porosity with the aged powder is in this case relatively minor compared to the increase of elongation caused by the coarser microstructure.

Overall, the main effect of the increased porosity in structures built with aged powder is a decrease of both yield tensile strength and ultimate tensile strength.

4.4. Outlook

Based on the results of this study, a hot gas extraction measurement could be used on a stored or recycled aluminium powder batch to determine its aging condition and what consequences to expect on the DED process when using this powder. A similar evaluation could be established with an absorbance measurement to assess the level of oxidation of a powder. Such a procedure could be applied to other processes, other aluminium alloys or other materials that are sensitive to oxidation and hydrogen pores, and which the properties during aging and recycling are of high interest.

In order to remedy to the ‘negative’ effects of using aged powder, one possibility would be to adapt the processing parameters

to the oxygen content in the powder. For a higher oxygen content, choosing a lower laser power could reduce the melt pool temperature and increase its surface tension to match the geometry of a track build with virgin powder. However, one limitation might be that a too low heat input can also induce lack of fusion and a higher porosity.

In some applications a high porosity is wanted, for instance for lightweight, permeability or osseointegration purposes [56–58]. Such porous metals can be manufactured by LPBF with a lower laser power and/or a higher scanning speed than the optimised parameters used to build dense material [58]. An additional option to tailoring the process parameters to obtain porous metals could then be to use aged powder instead of virgin powder in order to generate more porosity.

There are currently very few studies on mechanical properties of AlSi10Mg processed with DED, in [7] a maximal ultimate strength of 162 MPa was reported for the use of virgin powder, which is lower than the ultimate strength measured in the present work (208.6 ± 5.2 MPa). This difference of strength could be due to the different processing parameters chosen, or to the stress-relief treatment performed, but it clearly appears that more work should be carried out on the elementary properties of AlSi10Mg alloy processed with DED at different process parameters and heat treatments.

5. Conclusion

In this study, AlSi10Mg powder was aged in air in order to introduce higher contents of both Oxygen and Hydrogen. The following conclusions can be drawn on the use of aged aluminium powder in DED:

- The increased oxygen content of the powder leads to a decreased laser beam absorbance, likely because the oxide layer covering the particles is thicker and reflects more of the laser beam light
- During DED processing, the increased oxygen content in the powder most likely decreases the surface tension of the melt pool and increases its wetting on the substrate, which results in a track with a decreased height and an increased width
- Due to the lower track height, the heat input by the laser beam penetrates deeper into the substrate, resulting in an increased penetration depth
- Aging of powder induces more porosity in the tracks built, which is very likely due to hydrogen pores caused by the increased hydrogen content in the powder
- An increased porosity results in a lower tensile strength, while the presumably lower cooling rate induced by the higher penetration depth and the increased track overlap might lead to a coarser microstructure, which causes an increased elongation.

Declaration of Competing Interest

The authors declare that they have no known competing financial interests or personal relationships that could have appeared to influence the work reported in this paper.

Acknowledgments

The authors would like to express their gratitude towards the Division of Solid Mechanics at Luleå University of Technology for their collaboration on high-speed imaging. This study was accomplished within the European project SAMOA (no. 18079) funded by EIT Raw Materials.

Appendix A. Supplementary material

Supplementary data to this article can be found online at https://doi.org/10.1016/j.matdes.2022.110677.

References

[1] N.E. Prasad, R.J.H. Wanhill, Aerospace Materials and Materials Technologies, Springer Nature, Singapore (2017), https://doi.org/10.1016/b978-0-08-099925-8.00037-5.
[2] J. Hirsch, Recent development in aluminium for automotive applications, Trans. Nonferrous Met. Soc. China (English Ed. 24 (2014) 1995–2002. https://doi.org/10.1016/S1003-6326(14)63305-7.
[3] N.T. Aboulkhair, N.M. Everitt, I. Ashcroft, C. Tuck, Reducing porosity in AlSi10Mg parts processed by selective laser melting, Addit. Manuf. 1 (2014) 77–86, https://doi.org/10.1016/j.addma.2014.08.001.
[4] A. Hadadzadeh, B.S. Amirkhiz, J. Li, M. Mohammadi, Columnar to equiaxed transition during direct metal laser sintering of AlSi10Mg alloy: effect of building direction, Addit. Manuf. 23 (2018) 121–131, https://doi.org/10.1016/j.addma.2018.08.001.
[5] E. Brandl, U. Heckenberger, V. Holzinger, D. Buchbinder, Additive manufactured AlSi10Mg samples using Selective Laser Melting (SLM): microstructure, high cycle fatigue, and fracture behavior, Mater. Des. 34 (2012) 159–169, https://doi.org/10.1016/j.matdes.2011.07.067.
[6] M. Javidani, J. Arreguin-Zavala, J. Danovitch, Y. Tian, M. Brochu, Additive Manufacturing of AlSi10Mg Alloy Using Direct Energy Deposition: microstructure and Hardness Characterization, J. Therm. Spray Technol. 26 (2017) 587–597, https://doi.org/10.1007/s11666-016-0495-4.
[7] B. Chen, Y. Yao, X. Song, C. Tan, L. Cao, J. Feng, Microstructure and mechanical properties of additive manufacturing AlSi10Mg alloy using direct metal deposition, Ferroelectrics. 523 (2018) 153–166, https://doi.org/10.1080/00150193.2018.1392147.
[8] V.A. Muñoz, Analysis of the optimal parameters for 3D printing aluminum parts with a SLM 280 machine, 2017.
[9] K. Riener, S. Oswald, M. Winkler, G.J. Leichtfried, Influence of storage conditions and reconditioning of AlSi10Mg powder on the quality of parts produced by laser powder bed fusion (LPBF), Addit. Manuf. 39 (2021), https://doi.org/10.1016/j.addma.2021.101896 101896.
[10] P. Wei, Z. Wei, Z. Chen, J. Du, Y. He, J. Li, Y. Zhou, The AlSi10Mg samples produced by selective laser melting: single track, densification, microstructure and mechanical behavior, Appl. Surf. Sci. 408 (2017) 38–50, https://doi.org/10.1016/j.apsusc.2017.02.215.
[11] D. Buchbinder, H. Schleifenbaum, S. Heidrich, W. Meiners, J. Bültmann, High power Selective Laser Melting (HP SLM) of aluminum parts, in, Phys. Procedia, Elsevier B.V. (2011) 271–278, https://doi.org/10.1016/j.phpro.2011.03.035.
[12] M.A. Trunov, M. Schoenitz, E.L. Dreizin, Effect of polymorphic phase transformations in alumina layer on ignition of aluminium particles, Combust. Theory Model. 10 (2006) 603–623, https://doi.org/10.1080/13647830600578506.
[13] M. Mazur, Porosity in aluminium welds, Weld. Int. 6 (1992) 929–931, https://doi.org/10.1080/09507119209548317.
[14] D.M. Bauer, E. Schwarzenböck, I. Ludwig, N. Schupp, F. Palm, G. Witt, Investigations of aging behaviour for aluminium powders during an atmosphere simulation of the LBM process, Powder Metall. 60 (2017) 175–183, https://doi.org/10.1080/00325899.2017.1288841.
[15] K.L. Terrassa, J.C. Haley, B.E. MacDonald, J.M. Schoenung, Reuse of powder feedstock for directed energy deposition, Powder Technol. 338 (2018) 819–829, https://doi.org/10.1016/j.powtec.2018.07.065.
[16] I. Uslan, S. Saritas, T.J. Davies, Effects of variables on size and characteristics of gas atomized aluminum powders, Powder Metall. 42 (1999) 157–163, https://doi.org/10.1179/003258999665512.
[17] A. Ünal, Liquid break-up in gas atomization of fine aluminum powders, Metall. Trans. B. 20 (1989) 61–69, https://doi.org/10.1007/BF02670350.
[18] P. Moghimian, T. Poirié, M. Habibnejad-Korayem, J.A. Zavala, J. Kroeger, F. Marion, F. Larouche, Metal powders in additive manufacturing: a review on reusability and recyclability of common titanium, nickel and aluminum alloys, Addit. Manuf. 43 (2021) 102017.
[19] S. Ghods, R. Schur, E. Schultz, R. Pahuja, A. Montelione, C. Wisdom, D. Arola, M. Ramulu, Powder reuse and its contribution to porosity in additive manufacturing of Ti6Al4V, Materialia. 15 (2021) 100992.
[20] T. Fedina, J. Sundqvist, A.F.H. Kaplan, Spattering and oxidation phenomena during recycling of low alloy steel powder in Laser Powder Bed Fusion, Mater. Today Commun. 27 (2021), https://doi.org/10.1016/j.mtcomm.2021.102241 102241.
[21] A. Saboori, A. Aversa, F. Bosio, E. Bassini, E. Librera, M. De Chirico, S. Biamino, D. Ugues, P. Fino, M. Lombardi, An investigation on the effect of powder recycling on the microstructure and mechanical properties of AISI 316L produced by Directed Energy Deposition, Mater. Sci. Eng. A. 766 (2019), https://doi.org/10.1016/j.msea.2019.138360 138360.
[22] C. Paravan, A. Verga, F. Maggi, L. Galfetti, Accelerated ageing of micron- and nano-sized aluminum powders: metal content, composition and non-isothermal oxidation reactivity, Acta Astronaut. 158 (2019) 397–406, https://doi.org/10.1016/j.actaastro.2018.08.001.

[23] C.D. Boley, S.C. Mitchell, A.M. Rubenchik, S.S.Q. Wu, Metal powder absorptivity: modeling and experiment, Appl. Opt. 55 (2016) 6496, https://doi.org/10.1364/ao.55.006496.
[24] Y. Yan, L. Li, K. Sezer, D. Whitehead, L. Ji, Y. Bao, Y. Jiang, Experimental and theoretical investigation of fibre laser crack-free cutting of thick-section alumina, Int. J. Mach. Tools Manuf. 51 (2011) 859–870, https://doi.org/10.1016/j.ijmachtools.2011.08.004.
[25] A.E. Gheribi, P. Chartrand, Temperature and oxygen adsorption coupling effects upon the surface tension of liquid metals, Sci. Rep. 9 (2019) 1–9, https://doi.org/10.1038/s41598-019-43500-3.
[26] C.B. Eaker, M. Rashed Khan, M.D. Dickey, A method to manipulate surface tension of a liquid metal via surface oxidation and reduction, J. Vis. Exp. (2016 (2016)) 1–7, https://doi.org/10.3791/53567.
[27] C. Li, Y. Shi, Y. Gu, F. Yang, Effect of oxide on surface tension of molten metal, RSC Adv. 7 (2017) 53941–53950, https://doi.org/10.1039/c7ra11185a.
[28] H. Siva Prasad, F. Brueckner, A.F. Kaplan, Powder catchment in laser metal deposition, Journal of Laser Applications 31 (2) (2019).
[29] H. Siva Prasad, F. Brueckner, A.F.H. Kaplan, Powder incorporation and spatter formation in high deposition rate blown powder directed energy deposition, Addit. Manuf. 35 (2020), https://doi.org/10.1016/j.addma.2020.101413 101413.
[30] S.J. Wolff, H. Wang, B. Gould, N. Parab, Z. Wu, C. Zhao, A. Greco, T. Sun, In situ X-ray imaging of pore formation mechanisms and dynamics in laser powder-blown directed energy deposition additive manufacturing, Int. J. Mach. Tools Manuf. 166 (2021), https://doi.org/10.1016/j.ijmachtools.2021.103743 103743.
[31] Y. Zhang, Y. Guo, Y. Chen, Y. Cao, H. Qi, S. Yang, Microstructure and mechanical properties of Al-12Si alloys fabricated by ultrasonic-assisted laser metal deposition, Materials (Basel). 13 (1) (2020) 126.
[32] G.K.L. Ng, A.E.W. Jarfors, G. Bi, H.Y. Zheng, Porosity formation and gas bubble retention in laser metal deposition, Appl. Phys. A Mater. Sci. Process. 97 (2009) 641–649, https://doi.org/10.1007/s00339-009-5266-3.
[33] D.E.J. Talbot, Effects of hydrogen in aluminium, magnesium, copper, and their alloys, Int. Metall. Rev. 20 (1975) 166–184, https://doi.org/10.1179/imtlr.1975.20.1.166.
[34] C.E. Ransley, D.E.J. Talbot, Wasserstoff-Porosität in Metallen unter besonderer Berücksichtigung des Aluminiums und seiner Legierungen, International Journal of Materials Research 46 (5) (1955) 328–337.
[35] W.R. Opie, N.J. Grant, Hydrogen solubility in aluminum and some aluminum alloys, Jom. 2 (1950) 1237–1241, https://doi.org/10.1007/bf03399138.
[36] A. Eichenauer, W, Hattenbach, K, Pebler, Die Löslichkeit von Wasserstoff in festem und flüssigem Aluminium, Z. Met. 52 (1961).
[37] R.C. Atwood, P.D. Lee, Simulation of the three-dimensional morphology of solidification porosity in an aluminium-silicon alloy, Acta Mater. 51 (2003) 5447–5466, https://doi.org/10.1016/S1359-6454(03)00411-7.
[38] G.W. Mugica, D.O. Tovio, J.C. Cuyas, A.C. González, Julio César Cuyas, Effect of Porosity on the Tensile Properties of Low Ductility Aluminum Alloys, Mater. Res. 7 (2) (2004) 221–229.
[39] Shore R.J., McCauley R.B., Effects of Porosity on High Strength Aluminum 7039, in: Weld. Res. Suppl., Cleveland, United States, 1970: pp. 311–321.
[40] H. Mae, Comparative study of effect of porosity on tensile and shear ductility in A356 cast aluminum alloy by finite element simulation, Zair. Soc. Mater. Sci. Japan. 57 (2008) 1173–1178, https://doi.org/10.2472/jsms.57.1173.
[41] H. Mayer, M. Papakyriacou, B. Zettl, S.E. Stanzl-Tschegg, Influence of porosity on the fatigue limit of die cast magnesium and aluminium alloys, Int. J. Fatigue. 25 (2003) 245–256, https://doi.org/10.1016/S0142-1123(02)00054-3.
[42] Y.X. Gao, J.Z. Yi, P.D. Lee, T.C. Lindley, The effect of porosity on the fatigue life of cast aluminium-silicon alloys, Fatigue Fract. Eng. Mater. Struct. 27 (2004) 559–570, https://doi.org/10.1111/j.1460-2695.2004.00780.x.
[43] S.D. Jadhav, P.P. Dhekne, E. Brodu, B. Van Hooreweder, S. Dadbakhsh, J.P. Kruth, J. Van Humbeeck, K. Vanmeensel, Laser powder bed fusion additive manufacturing of highly conductive parts made of optically absorptive carburized CuCr1 powder, Mater. Des. 198 (2021), https://doi.org/10.1016/J.MATDES.2020.109369 109369.
[44] D. Zhang, R. Poprawe, F. Klocke, Entwicklung des Selective Laser Melting (SLM) für Aluminiumwerkstoffe, in (2004).
[45] M.R.M. Izawa, D.M. Applin, M.Q. Morison, E.A. Cloutis, P. Mann, S.A. Mertzman, Reflectance spectroscopy of ilmenites and related Ti and TiFe oxides (200 to 2500 nm): Spectral–compositional–structural relationships, Icarus. 362 (2021), https://doi.org/10.1016/J.ICARUS.2021.114423 114423.
[46] D. Zhang, W. Wang, Y. Guo, S. Hu, D. Dong, R. Poprawe, J.H. Schleifenbaum, S. Ziegler, Numerical simulation in the absorption behavior of Ti6Al4V powder materials to laser energy during SLM, J. Mater. Process. Technol. 268 (2019) 25–36, https://doi.org/10.1016/J.JMATPROTEC.2019.01.002.
[47] A. Da Silva, J. Volpp, A.F.H. Kaplan, The effects of laser irradiation on an aluminium powder stream in Directed Energy Deposition, Addit. Manuf. 41 (2021), https://doi.org/10.1016/j.addma.2021.101968 101968.
[48] J.Y. Tinevez, N. Perry, J. Schindelin, G.M. Hoopes, G.D. Reynolds, E. Laplantine, S. Y. Bednarek, S.L. Shorte, K.W. Eliceiri, TrackMate: an open and extensible platform for single-particle tracking, Methods. 115 (2017) 80–90, https://doi.org/10.1016/j.ymeth.2016.09.016.
[49] D. Ershov, M.-S. Phan, J.W. Pylvänäinen, S.U. Rigaud, L. Le Blanc, A. Charles-Orszag, J.R.W. Conway, R.F. Laine, N.H. Roy, D. Bonazzi, G. Duménil, G. Jacquemet, J.-Y. Tinevez, Bringing TrackMate into the era of machine-learning and deep-learning., BioRxiv. (2021) 2021.09.03.458852. https://www.biorxiv.org/content/10.1101/2021.09.03.458852v2%0Ahttps://www.biorxiv.org/content/10.1101/2021.09.03.458852v2.abstract.
[50] B. Brandau, A. Da Silva, F. Brueckner, A.F. Kaplan, Absorbance study of powder conditions for laser additive manufacturing, Materials & Design (2022).
[51] E. Glueckauf, G.P. Kitt, The hydrogen content of atmospheric air at ground level, Q. J. R. Meteorol. Soc. 84 (1958) 472–472. https://doi.org/10.1002/qj.49708436223.
[52] L.P.H. Jeurgens, W.G. Sloof, F.D. Tichelaar, E.J. Mittemeijer, Structure and morphology of aluminium-oxide films formed by thermal oxidation of aluminium, Thin Solid Films. 418 (2002) 89–101, https://doi.org/10.1016/S0040-6090(02)00787-3.
[53] L.P.H. Jeurgens, W.G. Sloof, F.D. Tichelaar, C.G. Borsboom, E.J. Mittemeijer, Determination of thickness and composition of aluminium-oxide overlayers on aluminium substrates, Appl. Surf. Sci. 144–145 (1999) 11–15, https://doi.org/10.1016/S0169-4332(98)00755-7.
[54] S. Kumari, S. Wenner, J.C. Walmsley, O. Lunder, K. Nisancioglu, Progress in Understanding Initiation of Intergranular Corrosion on AA6005 Aluminum Alloy with Low Copper Content, J. Electrochem. Soc. 166 (2019) C3114–C3123, https://doi.org/10.1149/2.0211911jes.
[55] J. Powell, D. Petring, R.V. Kumar, S.O. Al-Mashikhi, A.F.H. Kaplan, K.T. Voisey, Laser-oxygen cutting of mild steel: the thermodynamics of the oxidation reaction, J. Phys. D. Appl. Phys. 42 (1) (2009) 015504.
[56] F. Matassi, A. Botti, L. Sirleo, C. Carulli, M. Innocenti, Porous metal for orthopedics implants, Clin. Cases Miner. Bone Metab. 10 (2013) 111–115, https://doi.org/10.11138/ccmbm/2013.10.2.111.
[57] M.A. Atwater, L.N. Guevara, K.A. Darling, M.A. Tschopp, Solid State Porous Metal Production: a Review of the Capabilities, Characteristics, and Challenges, Adv. Eng. Mater. 20 (2018) 1–33, https://doi.org/10.1002/adem.201700766.
[58] R. Gotoh, B.I. Furst, S.N. Roberts, S. Cappucci, T. Daimaru, E.T. Sunada, Experimental and analytical investigations of AlSi10Mg, stainless steel, Inconel 625 and Ti-6Al-4V porous materials printed via powder bed fusion, Prog. Addit. Manuf. (2022), https://doi.org/10.1007/s40964-022-00269-8.